Membrane Binding by the Endophilin N-BAR Domain

Haosheng Cui, Gary S. Ayton, and Gregory A. Voth*
Center of Biophysical Modeling and Simulation, University of Utah, Salt Lake City, Utah

ABSTRACT The structure of the endophilin N-terminal amphipathic helix Bin/Amphiphysin/Rvs-homology (N-BAR) domain is unique because of an additional insert helix under the arch of the N-BAR dimer. The structure of this additional helix has not been fully resolved in crystallographic studies, and thus presents a challenge to molecular-level analysis. Large-scale molecular-dynamics simulations were therefore employed to investigate the interaction of a single endophilin N-BAR with a lipid bilayer. Various possible configurations of the additional insert helix under the top of the arch of the endophilin N-BAR were modeled to examine their effect on membrane bending. A residue-residue and residue-lipid headgroup distance analysis, similar to that performed with electron paramagnetic resonance spectroscopy, revealed that the insert helix remains perpendicular to the long axis of the N-BAR over the duration of the simulations. It was also found that the degree of membrane bending is directly related to the orientation of the additional insert helix, and that the perpendicular configuration generates the largest curvature consistent with mutation experiments. In addition, the angle formed between the two N-BAR monomers at the top of the arch is sensitive to the orientation of the insert helices. A membrane sensing-binding-bending mechanism is proposed to describe the process of an endophilin N-BAR interaction with a membrane.

INTRODUCTION

Bin/Amphiphysin/Rvs-homology (BAR) domains accumulate in neurons and are believed to play a key role in presynaptic endocytosis to recycle vesicles after neurotransmitter release (1–4). These crescent-shaped homodimers have positively charged residues on the concave surface (the ''arch'') and function in sensing and remodeling vesicle curvatures (2,5). In vitro, it has been observed that high concentrations of BAR domain dimers can tubulate vesicles with structured rings on the outer tubule (4,6). There is evidence from in vivo studies that they bind to membranes to form a variety of tubulated structures at the neck of clathrin-coated vesicles (5).

A BAR domain with an additional N-terminal amphipathic helix is denoted as an N-BAR domain (2,7,8). The N-terminal amphipathic helix has an α-helical structure that can be embedded in between the headgroups and tailgroups of the outer leaflet of a lipid bilayer when the N-BAR domain interacts with a membrane. This embedding results from the hydrophobic residues on one side of the helix and hydrophilic residues on the other (9–11). The amphipathic helices are unstructured in the solvent and only fold when they embed in the membrane, which makes it difficult to completely characterize their structure by crystallographic techniques (2).

The endophilin N-BAR domain is an important member of the BAR domain superfamily, which can be found in many stages of the endocytotic pathway from the initial curvature generation of vesicle budding to the late steps of vesicle uncoating (12,13). Recent studies have proposed several mechanisms whereby endophilin N-BAR domains can bend and remodel membranes (9,14). Moreover, via the SH3 domain, the endophilin protein module has the ability to recruit dynamin or synaptojanin, which acts as a membrane scissor or uncoater (12,15). Experimental work (9) has also suggested the possibility of a fast clathrin-independent endocytosis mediated only by endophilin N-BAR domains.

The structure of the endophilin N-BAR domain is characterized by two additional ''insert'' amphipathic helices (one on each monomer) located under the top of the ''arch'' of the N-BAR domain dimer. Like N-terminal amphipathic helices, they are also highly disordered in solution, but are believed to fold upon insertion into the upper membrane leaflet. Hereafter, they will be denoted as ''insert helices'' (14). The additional insert helices may not only allow endophilin N-BAR domains to induce larger curvatures compared to amphiphysin N-BAR domains and other BAR domain superfamily members (14), they also suggest the possibility of a different binding mechanism compared to amphiphysin (3). Several mutant experiments (9,14) have suggested that the N-BAR dimer rigidity is essential for membrane remodeling, so the additional insert helices may play an important role in maintaining the dimer association. It has also been observed that mutated endophilin BAR domains without the insert helices give rise to a significant decrease in membrane curvature (14). Thus it is still an open question as to how the insert amphipathic helices, in cooperation with scaffolding of the N-BAR domain protein (5), are involved in the overall membrane bending process.

Some structural information regarding the insert helix of the endophilin N-BAR domain has been revealed by crystallography (endophilin A1, Protein Data Bank (PDB) ID: 1X03; endophilin-III, PDB ID: 2Z0V), since they are unstructured in the solvent (9,14). Recent work using electron paramagnetic resonance (EPR) spectroscopy (9) showed that

Submitted July 28, 2009, and accepted for publication August 28, 2009.

*Correspondence: voth@hec.utah.edu

Editor: Peter Tieleman.

0006-3495/09/11/2746/8 $2.00

doi: 10.1016/j.bpj.2009.08.043

the amphipathic insert helices of N-BAR domains are parallel to the membrane surface; however, their orientation relative to the long axis of the N-BAR dimer was not resolved. Thus, to fully understand liposome remodeling and tubulation driven by endophilin N-BAR domains, a detailed molecular-level examination of the structure of the insert amphipathic helices is still required.

Molecular-dynamics (MD) simulations of membrane remodeling by amphiphysin N-BAR domains have provided considerable insights into N-BAR domain-mediated membrane sculpting (10,11,16). These simulations have shown that both the positively charged concave surface and the embedded amphipathic N-terminal helices are important for local membrane bending (10), and that the interaction between the N-BAR and the lipids needs to be sufficiently strong and correlated with the intrinsic membrane undulation frequencies (11). Possible oligomer arrangements for amphiphysin N-BARs at the coarse-grained MD level have been shown to induce a range of membrane curvatures (16,17). However, to our knowledge, no MD simulations of endophilin N-BARs have been performed to date.

Within the context of endophilin-induced membrane remodeling, MD simulations can provide important quantitative information on a very local level (e.g., averaged key residue-residue and residue-lipid headgroup distances that mirror such distances extracted from EPR measurements (18)), as well as at longer length scales (e.g., average membrane curvature as well as endophilin dimer structure). The combination of these simulation results may also provide considerable insight into the role and structure of the insert helices. The fact that the orientation of the insert helices is still not fully resolved experimentally motivated us to perform an MD simulation study involving the construction of different possible insert helix configurations, and to then examine the resulting membrane bending behavior. When combined with future experimental estimates, these simulation results will help to identify the most likely candidates for the orientation and structure of the insert helices.

In this work, we examined endophilin N-BAR-membrane interactions using a large-scale MD simulation similar in spirit to that used previously for amphiphysin (10,11). The next section describes some important simulation details, followed by the results, discussion, and a summary of our findings.

MATERIALS AND METHODS

The endophilin N-BAR domain coordinates (wild-type (WT) and mutant) were obtained from Masuda et al. (14) (PDB ID:1X03 and 1X04). The coordinates for an initially bent membrane (composed of 70%:30% dioleoylphosphatidylcholine (DOPC)/dioleoylphosphatidylserine (DOPS)) were obtained from the MD simulation of Blood and Voth (10) after 27 ns. For each system examined, the amphiphysin N-BAR domain in that configuration was then substituted by a single endophilin N-BAR domain at the same location, and the system was then resolvated, reionized, and reequilibrated.

Three systems (NBR-45, NBR-Perp, and NBR-Mut) containing different endophilin N-BAR domain structures were prepared from PDB 1X03 (Fig. 1, *a* and *b*) and PDB 1X04 (Fig. 1*c*) (14). NBR-Perp (Fig. 1*a*) has the insert helix perpendicular to the long axis of the N-BAR dimer, whereas NBR-45 (Fig. 1*c*) has the insert helix at 45° to the long axis. The mutant endophilin N-BAR domain, NBR-Mut (Fig. 1*b*), was constructed with the insert helices replaced by a helical stretch previously obtained from experiment (14). The design of the three systems follows from observations from previous studies (10) in which the N-terminal helices were placed perpendicular to the BAR. In all systems, both the insert helices and the N-terminal helices are embedded parallel to the membrane surface such that the hydrophobic residues of the amphipathic helices are associated with tailgroups of the lipids, whereas the hydrophilic parts of amphipathic helices are closer to the lipid headgroups and surrounding solvent. Because all of the amphipathic helices had to be embedded in the outer bilayer leaflet from the outset without overly stressing the endophilin dimer, a prebent membrane obtained from a previous amphiphysin N-BAR result (10) for endophilin was employed.

All three systems (NBR-45, NBR-Perp, and NBR-Mut) were identically prepared. The membranes were solvated, top and bottom, by a minimum

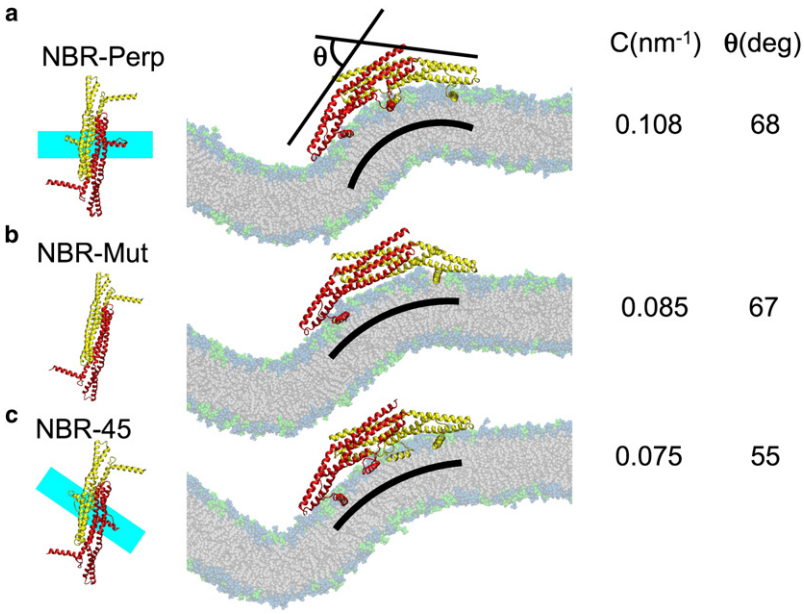

FIGURE 1 MD simulation snapshots of the (*a*) NBR-Perp, (*b*) NBR-Mut, and (*c*) NBR-45 systems (see text for details). The snapshot on the far left highlights the location of the arch helix in the different systems. The center panel shows the induced membrane curvature for the three systems, with the curvature for NBR-Perp being the largest and that for NBR-45 the smallest. The actual average curvatures calculated over the last 55 ns of a 75 ns simulation are also reported. The SD of the curvature was calculated by dividing this time interval into five blocks each of 11 ns, and it was found that the error was within 0.01 nm^{-1}. The angle θ (shown in panel *a*) is defined from the first parts of helix-3 (residues 180–195) of the dimer, and gives a measure of the "arch" of the endophilin dimer on average. NBR-45 exhibits a significant drop in the value of θ, whereas NBR-Perp and NBR-Mut maintain their initial structure over the course of the simulation. Employing the method described above for error estimation, the error of this calculation is within $\pm 3°$.

15 Å layer of TIP3P explicit waters, and 0.15 M NaCl was included to maintain charge neutrality (19). The dimensions of the systems reached 446 × 86 × 163 Å^3 (i.e., ~702,530 atoms).

The CHARMM22 (20) force field was employed for the protein parameters, and the CHARMM27 (21) force field determined the lipid and lipid protein parameters. Long-range electrostatic interactions were computed using the particle mesh Ewald algorithm (22) with standard periodic boundary conditions. SHAKE/SETTLE algorithms (23,24) were used to constrain all atom-hydrogen bonds, thus allowing for a time step of 2 fs. A conjugate-gradient minimization of 80,000 time steps was initially applied and the backbone atoms of the N-BAR domains and the phosphate atoms of the lipids were restrained with harmonic potentials with spring constants of 100 kcal/(mol Å^2). The systems were then heated to 310 K with the same restraints. Initial constant-pressure, constant-temperature (NPT) equilibrations gradually reduced the restraint potentials on the C_α atoms (e.g., 200 ps with spring constants of 10 kcal/(mol Å^2), and then 200 ps of 1 kcal/(mol Å^2)). To fully maximize the interaction of the amphipathic helices with the lipids while also maintaining their helical structure, additional equilibrations (6 ns) having harmonic potential restraints with spring constants of 0.5 kcal/(mol Å^2) on the C_α atoms of the amphipathic helices were performed. This was followed by fully unconstrained, fully anisotropic pressure coupling NPT MD simulations at 1 atm and 310 K. Damping coefficients of Langevin thermostats in the NPT algorithm were set to 0.5 ps^{-1} and the Langevin-piston barostats were set with a 2 ps piston period and a 2 ps damping time (25). All MD simulations were performed using the NAMD simulation package (26), and analysis and visualizations were conducted with the VMD package (27).

RESULTS

Key residue distance measurements

When the endophilin dimer is in contact with the membrane, its average structure relative to the original crystal structure can be examined by calculating the average residue-residue and residue-phosphate atom distances, and employing the C_α atoms of the residues along with the location of the first peak in the corresponding radial distribution function (RDF). These distances could, in principle, also be measured with EPR spectroscopy (9). In Fig. 2, a simulation snapshot of the endophilin dimer is shown, with key residues depicted in darker colors for clarity. The green arc gives an indication of the average location of the phosphate atoms in the membrane, and the blue and red arrows respectively denote the closest and farthest residues from the phosphate atoms in the bilayer. It should be noted that these lines are drawn to guide the eye only, as the actual measurement requires averaging over instantaneous fluctuations. The black arrows refer to key residue-residue distances for identical residues found in each monomer (e.g., residues Lys-227, Pro-62, Ala-63, Ala-96, Ser-216). The final dotted line gives the distance between residues Ser-200 and Leu-166 for further comparison. The final distances are given in Tables 1 and 2. On average, the structure of the dimer relative to the original crystal structure is maintained. The variation in distances between the membrane and the protein demonstrates the importance of the N-terminal amphipathic helices in restraining the membrane such that it maintains a close proximity to the protein. Of interest, the residues closest to the N-terminal helices are closest to the membrane; residues underneath the BAR domain arch are generally farther away. The insert helices thus may play a role in modulating the distance between the protein and membrane in generating a smooth (rather than kinked) membrane curvature as shown in Fig. 1.

The average insertion depth of an insert helix can also be examined. In Fig. 3, the average depth of one of the insert helices is shown, starting from residue 63 and ending at the N-terminal residue 79. The shaded yellow region gives the approximate location of the headgroup region of the bilayer in the vicinity of the insert helices. The majority of the gray hydrophobic residues on average reside in the lipid tail region of the membrane, whereas the green hydrophilic residues generally reside in the upper region of the phosphate headgroups. Of interest, the insert helix ''rises'' out of the membrane in going from residue 63 to 79, until the N-terminal region partially resides out of the bilayer and is exposed to the surrounding solvent. The origin of this effect appears to be related to the fact that the residues are more hydrophilic in the end-terminal region.

The stability of the NBR-Perp system can be examined by measuring key residue-residue distances in opposing insert helices, as shown in the upper snapshot in Fig. 4. The component of the projected distance orthogonal to the long axis of the N-BAR dimer is reported in this analysis. If, over the course of the simulation, the system had exhibited

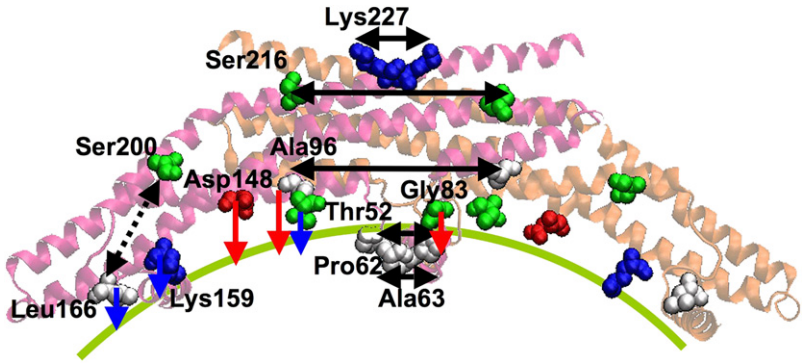

FIGURE 2 Residue-residue and residue-phosphate atom distances from the MD simulation. The image at the top is a simulation snapshot of the endophilin dimer. The arc (*green* online) gives the approximate average location of the phosphate atoms in the lipid headgroups. The arrows (*black* online) designate the residue-residue distances for like residues in each monomer (residues Lys-227, Pro-62, Ala-63, Ala-96, Ser-216). The dotted line designates the distance between residues Ser-200 and Leu-166. The final distances are given in Table 1. Distances from residues to the average location of the closest phosphate atom in the lipid headgroups (denoted by the *vertical lines*) are given in Table 2. The residues closest to the phosphate headgroups are Thr-52, Lys-159, and Leu-166 (with distances designated by the *vertical arrows*), and Gly-83, Ala-96, and Asp-148 (with distances denoted by the *arrows*) are the farthest away.

TABLE 1 Dimer residue distances

Residue	PDB (Å)	MD (Å)
227	7	9
62	10	10
63	10	9
96	36	36
216	34	35
166–200	21	21

PDB distances were found from the original PDB structure, the MD simulation results employed the C_α atoms of corresponding residues, and the average distances were measured from the first peak of the RDF over 75 ns of simulation. The errors of the distance results in this table fall within ± 0.2 Å; the error was estimated by calculating the standard deviation (SD) of the averaged distances for each residue over 15 ns trajectory blocks over the entire simulation trajectory.

TABLE 2 Residue-closest phosphate atom distances

	NBR-Perp	NBR-45
Residue	Dist. (Å)	Dist. (Å)
52	7	9
83	13	9
96	14	12
148	11	12
159	8	6
166	6	8

NBR-Perp and NBR-45 correspond to the perpendicular and diagonal helix configurations. The errors of the distance results in this table fall within ± 0.2 Å; the error was estimated by calculating the SD of the averaged distances for each residue over 15 ns trajectory blocks over the entire simulation trajectory.

a tendency to adopt configurations in which the insert helices were not antiparallel and approximately perpendicular to the long axis of the endophilin N-BAR dimer, the projected orthogonal residue-residue distances would have picked that up. For example, if the embedded helices were at some angle $<90^\circ$ to the long axis of the N-BAR dimer, the average component of the projected distance between the residues orthogonal to the long axis of the N-BAR dimer would be less than that expected if the helices adopted an arrangement that was more perpendicular to the long axis of the dimer. However, as can been seen from Table 3, the resulting distances for the NBR-Perp are consistent with an antiparallel and perpendicular configuration on average. Likewise, the NBR-45 system exhibits a structure wherein the insert helices maintain a nonperpendicular arrangement. It should be noted that these distance measurements, like those presented in Fig. 2, could also be measured with EPR spectroscopy.

Varying insert helix orientations

As described above, three different insert helix configurations were tested (NBR-Perp, NBR-Mut, and NBR-45; see Fig. 1). Returning to the results in Fig. 1, we can examine the resulting membrane curvature after 75 ns of simulation for the three different systems. The largest membrane curvature is that for the NBR-Perp system (Fig. 1*a*), followed by the NBR-Mut system (Fig. 1*b*) and then the NBR-45 system (Fig. 1*c*). In Fig. 1*a*, the embedded insert helices can be clearly seen in the snapshot of the membrane. The combination of the insert helices, along with the other two N-terminal amphipathic helices, resembles three parallel cylinders that each embed in the upper leaflet. This concerted effect acts to increase the local mass density underneath the arch of the dimer such that the membrane readily bends. The NBR-Mut system does not have this additional helix and must rely on electrostatic interactions alone underneath the arch to maintain the curvature. The NBR-45 system, with the smallest curvature, has the insert helix in a nonparallel orientation relative to the other two N-terminal amphipathic helices. Given that this system is the same as the NBR-Perp system except for the orientation of this helix, it is surprising that just varying the orientation of the insert helix can result in such a suppressed membrane curvature. Presumably, the parallel configuration of insert helices generates membrane curvature in a concerted fashion. It is reasonable to assume that the directionality of the induced membrane curvature, due to amphipathic helix insertion, would be roughly perpendicular to the helix orientation. In the NBR-Perp system, the resulting generated curvature is amplified, whereas for the NBR-45 system, there is a cancellation effect due to the nonparallel arrangement of the helices.

All three N-BARs remained upright on the membrane during the course of the MD simulations. In the case of the NBR-Perp and NBR-45 systems, this may due to the additional support supplied by the insert helix. It may also be due to the fact that the simulations were started from a prebent membrane. This can be contrasted with the results of amphiphysin N-BAR simulations (e.g., the NBR1 system from Blood and Voth (10)) in which the BAR dimer can fall over on the membrane. It would therefore be interesting to investigate a mutated endophilin with one side of the helices cleaved or significantly truncated to explore whether the amphipathic helices are critical for restraining the N-BAR perpendicular to the membrane.

All three systems retained the curvatures from the initial configurations (within the effects of thermal fluctuations). The endophilin N-BAR domain with perpendicular insert helices induced the largest curvature (the arc generated underneath the arch is closer to an arc of a circle). Conversely, the NBR-Mut snapshot exhibits a flat membrane region at the center of the BAR dimer, whereas the NBR-45 snapshot exhibits low curvature region around the end of the BAR. Fig. 5 shows an analytical curvature calculation indicating that, as expected, the NBR-Perp system generated the largest membrane curvature, followed by the NBR-Mut system and then the NBR-45 system. This result directly shows that, at least for one-dimensional curvature generation (e.g., tubulated vesicles), the existence of insert helices will increase the membrane bending only when they are in an

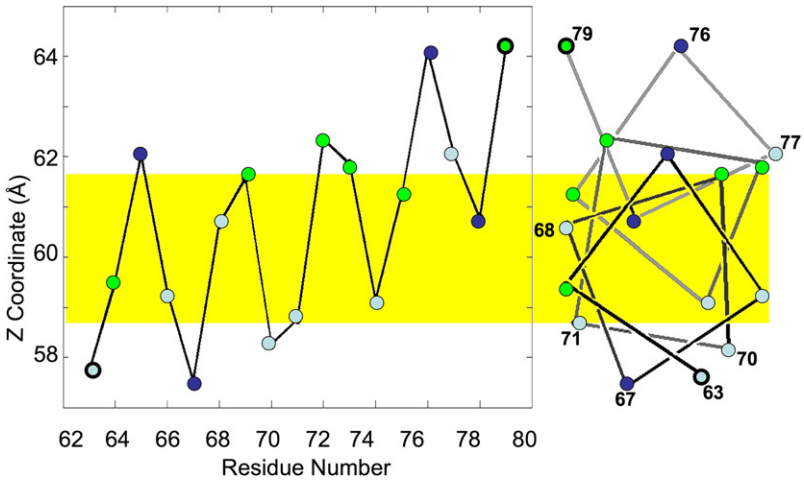

FIGURE 3 (*Left panel*) Average helix depth in the lipid bilayer found by averaging the coordinates of the C_α atoms on the helix (residues 63–79) in the MD simulation. The shaded bar (*yellow* online) gives the range of the location of nearby phosphate headgroups in the bilayer. Gray (*gray* online) sites are hydrophobic, dark gray (*green* online) are hydrophilic, and the darkest (*blue* online) are charged. The terminal end of the helix (residues 73–79) exhibits a distinct rising out of the membrane. The periodicity is ~3.6 amino acids per turn. (*Right panel*) An ''end-on'' view showing how the turns of the helix are arranged.

orientation that is perpendicular to the BAR domain arch long axis. For orientations of the insert helix that are not perpendicular to the long axis of the BAR, the insert helix may impede membrane remodeling. The membrane underneath the arch of the NBR-Mut system is nearly flat due to the mutated helical stretch, whereas the NBR-Perp and NBR-45 systems with the insert helices generated more smoothly curved membranes. This could indicate a possible role of the endophilin insert helices in smoothing out the induced membrane curvature.

Structural changes of the BAR dimer itself can be assessed by examining the angle θ between the residues of helix 3 (residues 180–195) for each of the monomers, which in turn gives an indication of the angle between the two monomers (28) (see Fig. 1). In Fig. 6, it is shown that θ for the NBR-Mut and NBR-Perp systems remained constant during the course of the simulation, whereas NBR-45 exhibited a decrease. This result suggests another reason for the low curvature generated by the NBR-45 system: the actual angle of the dimer has decreased. In addition to the more familiar idea of BAR domains bending the membrane, it could also be possible that the membrane, under certain circumstances, can in turn deform BAR domain proteins. This may lead to a dissociation of the dimer at longer timescales. The results support the idea that dimer rigidity is related to, and essential for, membrane remodeling (14).

SUMMARY AND CONCLUSIONS

In recent experimental work (14), the curvatures of membrane tubules induced by interactions with WT endophilin (PDB ID:1X03) and an endophilin mutant (PDB ID: 1X04) were compared. In those experiments it was observed that the mutant endophilin without the insert helices formed tubules with significantly smaller curvatures than the WT. The MD simulation results reported here suggest that the NBR-Perp system generates the largest curvature compared to the two other types of endophilin N-BARs, including NBR-Mut (see Fig. 1). Thus, it is predicted that the perpendicular conformation of the insert helices is the most likely conformation for membrane-bound WT endophilin N-BARs (in contrast to the first few residues of the helix in the crystal structure (PDB ID: 1X03 and 2Z0V), which indicate a possible 45° orientation). The membrane curvatures

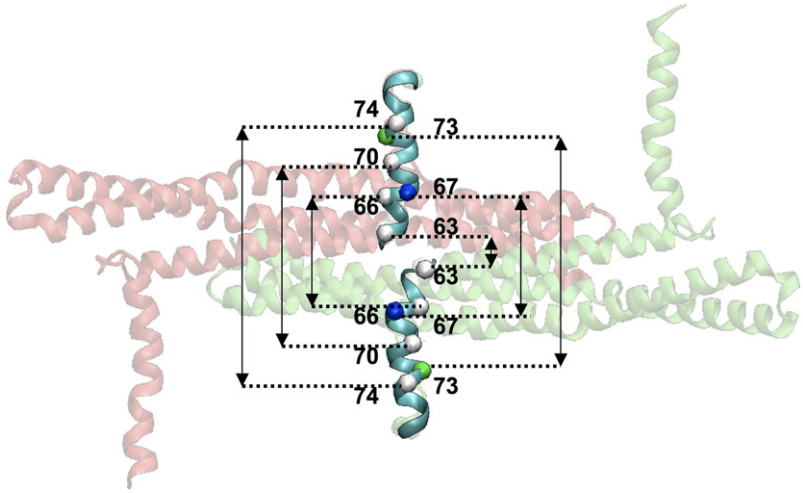

FIGURE 4 Projected distance orthogonal to the long axis of the N-BAR dimer (denoted by the *black arrows*) between identical residues of the two insert helices (shown in high resolution, superimposed over the entire endophilin dimer). The dotted black lines designate the residue numbers. These are calculated from the MD simulation results from the location of the first peak of corresponding RDF between the C_α atoms of like residues (shown in Table 3.). In the NBR-Perp case, the projected distances increase with increasing residue number, indicating an antiparallel arrangement of the helices that is perpendicular to the long axis of the N-BAR. In the NBR-45 system, the projected distance is less, indicating that the insert helices are not orthogonal to the long axis of the N-BAR.

TABLE 3 Projected distances between insert helix residues

	NBR-Perp	NBR-45
Residue	Dist. (Å)	Dist. (Å)
64	11	11
65	16	12
66	18	10
67	22	16
70	30	20
71	34	27
73	37	26
74	42	31
75	45	36
77	49	38
78	53	44
79	55	43

Errors of all of the distance results in this table fall within ±0.4 Å; the error was estimated by calculating the SD of the averaged distances for each residue over 15 ns trajectory blocks over the entire simulation trajectory.

generated in these single endophilin N-BAR domain MD simulations thus favor insert helices with a perpendicular orientation relative to the long axis of the BAR domain. However, this scenario may be altered in cases in which endophilin N-BAR domains bind to real liposomes with two curvature components. Indeed, it may be possible that the orientation of the insert helices may modulate the membrane binding over different curvatures (9). Furthermore, it is known from experiment (2) that endophilin N-BAR domains exist in a state of monomer-dimer equilibrium in vivo. On top of that, the resulting orientation of the insert helices (the structural details of the unfolded state in the monomer

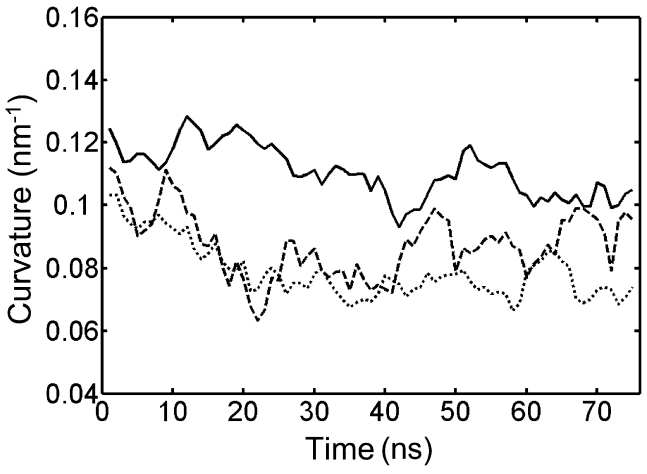

FIGURE 5 Membrane curvatures as a function of time in the MD simulations for the three systems: NBR-45 (*dotted line*), NBR-Perp (*solid line*), and NBR-Mut (*dashed line*). The NBR-Perp holds the largest curvature, and the NBR-45 has a slightly larger overall curvature compared to NBR-Mut. Overall, membranes bent by endophilin show lower local curvatures than those in amphiphysin N-BAR systems (the latter having a curvature ~0.15 nm^{-1}), even though endophilin N-BARs appear to result in tubulated membrane structures with a higher overall degree of curvature than amphiphysin (14). Curvature was calculated by fitting the coordinates of the outer leaflet lipids phosphate atoms in positively curved areas to a circle.

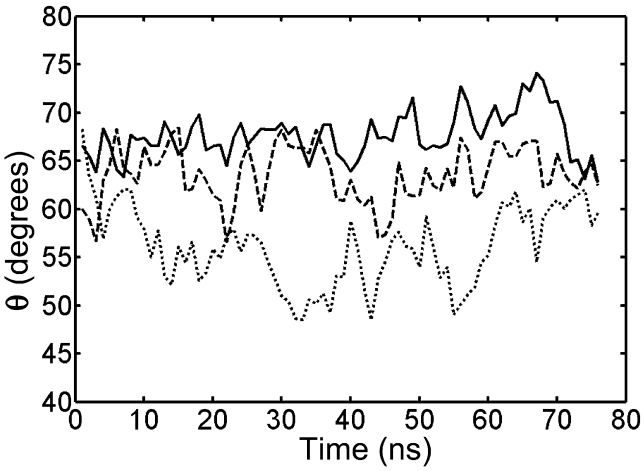

FIGURE 6 Angle θ between the first parts of helix-3 (residues 180–195) of the N-BAR dimer for the three systems: NBR-45 (*dotted line*), NBR-Perp (*solid line*), NBR-Mut (*dashed line*). NBR-45 had a significant drop in θ, whereas NBR-Perp and NBR-Mut retained their initial structure.

are not yet well known) further complicates the overall dynamical equilibrium of endophilin. The number of possible orientations observed under experimental conditions is much greater than the number of distinct cases presented here. Though no orientational changes were found during the course of simulations, it is possible that the insert helices of endophilin can undergo conformation changes to better interact with the membrane on longer timescales. To shed some light on the relative free-energy differences between the different insert helix states, it would be very interesting to calculate the relative free energies for different states of endophilin (e.g., the free-energy profile along a coordinate connecting the different insert helix conformations). This will be investigated in future studies.

It is also useful to compare the ''shape'' of the bent membrane underneath different N-BAR domains. In previous amphiphysin N-BAR domain simulations (10), a significant local membrane curvature, together with a strong electrostatic interaction between the BAR inner surface residues and lipid headgroups, was observed under the arch of the BAR domain. In the NBR-Mut system, the lipid bilayer is relatively flat under the arch of the dimer due to the mutated helical stretch. In contrast, in the NBR-Perp system, which includes the insert helices, the membrane has a smoother and more rounded membrane curvature. It is interesting to note that the local membrane curvature of the NBR-Perp system at the center of the BAR dimer is smaller than the previous amphiphysin N-BAR simulation result. However, in vitro, endophilin N-BAR domains generally tubulate vesicles into a smaller diameter compared to amphiphysin N-BAR domains (14). Amphiphysin N-BAR domains may rely more on electrostatic interactions to maintain the curvature under their arch, and this interaction may not be strong enough to overcome the nonlocal membrane curvature generated by other N-BAR domains in the vicinity. The

endophilin N-BAR domains, on the other hand, with the additional insert helices, could better stabilize the local membrane curvature. In addition, the density of the amphipathic helices may play a critical role when more than a single N-BAR domain is involved (11). With two additional amphipathic helices under the top of the arch, endophilin N-BAR domains have twice the helix density, which in turn may lead to more significant tubulation behavior. Moreover, previous work has shown that fluctuations of the BAR domain relative to its average structure can have a large impact on membrane remodeling (11). With the additional support from the insert helices, no significant structural fluctuations of endophilin relative to the long axis of the BAR were observed in the MD simulations presented here. This could additionally facilitate endophilin N-BAR domains in stabilizing a bent membrane. These observations are also in agreement with experimental results from a previous study on endophilin-recruiting dynamins (3). In that work, it was determined that endophilin can stabilize tubules from dynamin disturbances, but amphiphysin cannot.

Therefore, we propose a possible membrane remodeling mechanism of endophilin N-BAR domains: the ''sensing-binding-bending'' mechanism. The sensing component involves an initial membrane thermal undulation or other local deformation (e.g., one caused by another protein module, such as the epsin ENTH domain) coupling with the N-BAR concave surface via electrostatic interactions with the negatively charged lipid headgroups. The binding component is then coupled with the resulting density variations in the inner and outer leaflets (possibly enhanced by the BAR-lipid headgroup interactions) and facilitates the formation and insertion of folded N-terminal amphipathic helices into the lower-density regions of the membrane outer leaflet. The bending component arises as the N-terminal amphipathic helices embed and fully stabilize in the outer leaflet of the membrane. In this mechanism, the electrostatic interactions between the BAR domain and the lipid headgroups favor membrane bending, but they do not primarily drive the membrane remodeling process. (Note that the orientation of the insert helices for endophilin N-BAR domains may depend on the local curvature of the membrane, e.g., one-dimensional versus two-dimensional as discussed above.) This locally generated curvature will then induce an additional lipid density asymmetry in the proximity of the N-BAR domain, and thus additional N-BAR domains will be attracted to initiate another sensing-binding-bending sequence. Additional oligomerization interactions between the N-BAR domains will lead to more extended remodeled membrane structures, such as long tubules. However, the endophilin N-BAR sensing-binding-bending mechanism suggests that such perfect tubulated membrane structures will be more the exception than the rule, and that more complex ''reticulated'' or ''web-like'' structures may instead be more prevalent for remodeled liposomes from in vitro experiments. This suggestion is consistent with recent results from both mesoscopic simulations and electron microscopy experiments (29).

We have explored the local interactions of endophilin N-BAR domains with membranes, and discussed the possible implications for larger-scale membrane remodeling processes based on these findings. We found that the orientation of the additional endophilin N-BAR insert helix plays a key role in the degree of local membrane bending. Moreover, the perpendicular orientation of the insert helix relative to the long axis of the N-BAR dimer is predicted to be the preferred orientation when it is bound to the membrane. The coordinated effort of multiple N-BAR amphipathic helices may not only modulate the degree of local membrane curvature, it may also affect how smoothly bent the membrane is underneath the arch of the dimer. Detailed residue-residue and residue-headgroup measurements from the MD simulations further support the notion that the perpendicular configuration of the additional insert helix is its most likely preferred orientation. Future comparisons of these simulation-derived parameters with experimental results from, e.g., EPR spectroscopy (R. Langen, University of Southern California, personal communication, 2009) will provide additional insight into the membrane binding and bending mechanism of endophilin N-BAR domains.

We thank Richard Swenson and Dr. Phil Blood for very helpful suggestions and for providing data from earlier work. Computational resources were provided by the National Science Foundation through the TeraGrid computing resources of the Texas Advanced Computing Center, the Pittsburgh Supercomputing Center, the San Diego Supercomputing Center, and the National Institute for Computational Sciences.

This work was supported by the National Institutes of Health (GM063796).

REFERENCES

1. Schmidt, A., M. Wolde, C. Thiele, W. Fest, H. Kratzin, et al. 1999. Endophilin I mediates synaptic vesicle formation by transfer of arachidonate to lysophosphatidic acid. *Nature*. 401:133–141.
2. Peter, B. J., H. M. Kent, I. G. Mills, Y. Vallis, P. J. G. Butler, et al. 2004. BAR domains as sensors of membrane curvature: the amphiphysin BAR structure. *Science*. 303:495–499.
3. Farsad, K., N. Ringstad, K. Takei, S. R. Floyd, K. Rose, et al. 2001. Generation of high curvature membranes mediated by direct endophilin bilayer interactions. *J. Cell Biol.* 155:193–200.
4. Takei, K., V. I. Slepnev, V. Haucke, and P. De Camilli. 1999. Functional partnership between amphiphysin and dynamin in clathrin-mediated endocytosis. *Nat. Cell Biol.* 1:33–39.
5. McMahon, H. T., and J. L. Gallop. 2005. Membrane curvature and mechanisms of dynamic cell membrane remodelling. *Nature*. 438:590–596.
6. Frost, A., R. Perera, A. Roux, K. Spasov, O. Destaing, et al. 2008. Structural basis of membrane invagination by F-BAR domains. *Cell*. 132:807–817.
7. Gallop, J. L., and H. T. McMahon. 2005. BAR domains and membrane curvature: bringing your curves to the BAR. *Biochem. Soc. Symp.* 72:223–231.
8. Fernandes, F., L. M. S. Loura, F. J. Chichon, J. L. Carrascosa, A. Fedorov, et al. 2008. Role of helix-0 of the N-BAR domain in membrane curvature generation. *Biophys. J.* 94:3065–3073.

9. Gallop, J. L., C. C. Jao, H. M. Kent, P. J. Butler, P. R. Evans, et al. 2006. Mechanism of endophilin N-BAR domain-mediated membrane curvature. *EMBO J.* 25:2898–2910.

10. Blood, P. D., and G. A. Voth. 2006. Direct observation of Bin/amphiphysin/Rvs (BAR) domain-induced membrane curvature by means of molecular dynamics simulations. *Proc. Natl. Acad. Sci. USA.* 103:15068–15072.

11. Blood, P. D., R. D. Swenson, and G. A. Voth. 2008. Factors influencing local membrane curvature induction by N-BAR domains as revealed by molecular dynamics simulations. *Biophys. J.* 95:1866–1876.

12. Ringstad, N., H. Gad, P. Low, G. Di Paolo, L. Brodin, et al. 1999. Endophilin/SH3p4 is required for the transition from early to late stages in clathrin-mediated synaptic vesicle endocytosis. *Neuron.* 24:143–154.

13. Gad, H., N. Ringstad, P. Low, O. Kjaerulff, J. Gustafsson, et al. 2000. Fission and uncoating of synaptic clathrin-coated vesicles are perturbed by disruption of interactions with the SH3 domain of endophilin. *Neuron.* 27:301–312.

14. Masuda, M., S. Takeda, M. Sone, T. Ohki, H. Mori, et al. 2006. Endophilin BAR domain drives membrane curvature by two newly identified structure-based mechanisms. *EMBO J.* 25:2889–2897.

15. Schuske, K. R., J. E. Richmond, D. S. Matthies, W. S. Davis, S. Runz, et al. 2003. Endophilin is required for synaptic vesicle endocytosis by localizing synaptojanin. *Neuron.* 40:749–762.

16. Arkhipov, A., Y. Yin, and K. Schulten. 2008. Four-scale description of membrane sculpting by BAR domains. *Biophys. J.* 95:2806–2821.

17. Yin, Y., A. Arkhipov, and K. Schulten. 2009. Simulations of membrane tubulation by lattices of amphiphysin N-BAR domains. *Structure.* 17:882–892.

18. Jao, C. C., B. G. Hegde, J. Chen, I. S. Haworth, and R. Langen. 2008. Structure of membrane-bound α-synuclein from site-directed spin labeling and computational refinement. *Proc. Natl. Acad. Sci. USA.* 105:19666–19671.

19. Jorgensen, W. L., J. Chandrasekhar, and J. D. Madura. 1983. Comparison of simple potential functions for simulating liquid water. *J. Chem. Phys.* 79:926–935.

20. MacKerell, A. D., D. Bashford, M. Bellott, R. L. Dunbrack, J. D. Evanseck, et al. 1998. All-atom empirical potential for molecular modeling and dynamics studies of proteins. *J. Phys. Chem. B.* 102:3586–3616.

21. Feller, S. E., and A. D. MacKerell. 2000. An improved empirical potential energy function for molecular simulations of phospholipids. *J. Phys. Chem. B.* 104:7510–7515.

22. Essmann, U., L. Perera, M. L. Berkowitz, T. Darden, H. Lee, et al. 1995. A smooth particle mesh Ewald method. *J. Chem. Phys.* 103:8577–8593.

23. Allen, M. P., and D. J. Tildesley. 1989. Computer Simulation of Liquids. Oxford University Press, Oxford, UK.

24. Miyamoto, S., and P. A. Kollman. 1992. Settle: an analytical version of the SHAKE and RATTLE algorithm for rigid water models. *J. Comput. Chem.* 13:952–962.

25. Feller, S. E., Y. Zhang, R. W. Pastor, and B. R. Brooks. 1995. Constant pressure molecular dynamics simulation: the Langevin piston method. *J. Chem. Phys.* 103:4613–4621.

26. Phillips, J. C., R. Braun, W. Wang, J. Gumbart, E. Tajkhorshid, et al. 2005. Scalable molecular dynamics with NAMD. *J. Comput. Chem.* 26:1781–1802.

27. Humphrey, W., A. Dalke, and K. Schulten. 1996. VMD: visual molecular dynamics. *J. Mol. Graph.* 14:33–38, 27–28.

28. Wang, Q., H. Y. K. Kaan, R. N. Hooda, S. L. Goh, and H. Sondermann. 2008. Structure and plasticity of endophilin and sorting nexin 9. *Structure.* 16:1574–1587.

29. Ayton, G. S., E. Lyman, V. Krishna, R. Swenson, C. Mim, et al. 2009. New insights into BAR domain induced membrane remodeling. *Biophys. J.* 97:1616–1625.